



# Optimization of Selective Laser Melting Process Parameters for Enhanced Mechanical Properties and Friction Behavior of AlFeSi10Mg Alloy Components

Madhurima Kalluru<sup>1\*</sup>, Dr.K.Devaki Devi <sup>2</sup>

<sup>1\*</sup>Research scholar of JNTUA, Mechanical Department, GPREC Research Centre, Kurnool, AP, India.

<sup>2</sup>Associate Professor, Mechanical Department, GPREC, Kurnool, AP, India. E-mail: madhurimakalluru77@gmail.com E-mail: devakidevik.me@gprec.ac.in

**Citation:** Madhurima Kalluru et.al (2023), Optimization of Selective Laser Melting Process Parameters for Enhanced Mechanical Properties and Friction Behavior of AlFeSi10Mg Alloy Components., Educational Administration: Theory And Practice, 29(4), 1288-1299

Doi: 10.53555/kuey.v29i4.4889

## ARTICLE INFO

## ABSTRACT

This research investigates wear characteristics of an AlFeSi10Mg alloy produced through selective laser melting (SLM), while introducing a layer-by-layer additive process simulation to streamline the SLM printing process, thereby saving time, cost, and material. AM simulation results demonstrate reduced displacement and temperature during SLM printing. The study emphasizes the critical role of build orientation in determining the quality and performance of AM parts. Employing an L16 orthogonal array of Taguchi design experiments, a model is developed for wear characterization. Optimal process parameters are identified for achieving low wear rate, high density, and high hardness. At the optimal condition (T5), wear measurements include a depth of 94 micrometers, a length change of 0.06%, a volume of 1.25 mm<sup>3</sup>, a velocity of 1674.46 mm/s, a wear rate of 4.97×10<sup>-8</sup> mm<sup>2</sup>/N, a coefficient of 0.04 mm<sup>2</sup>/N, and a frictional force of 14.1 N. Laser energy density is computed as 150 J/mm<sup>3</sup> based on the achieved optimal parameters.

**Keywords:** Laser Powder Bed Fusion (LPBF), Selective Laser Melting (SLM), AlFeSi10Mg alloy, Wear Characterization, Microstructure, Hardness, Density.

## INTRODUCTION

Selective laser melting (SLM) is a technique that may be used to make components layer by layer out of metal powder. On a simple chamber plate, the component is manufactured using Selective Laser Melting (SLM). Each layer is formed by sweeping the laser's intensity along the XY axis. To facilitate the deposit of the next layer of powder, the piston is lowered after each layer is scanned. The iterative approach is performed until the component is completed. During peak and off-peak hours, the SLM process takes longer. The primary objective during peak hours is to liquefy the powder layer; the addition of powder and the reduction of substrate require time. Surface laser melting commonly utilises a pulverised aluminium alloy with unique properties such as low viscosity, light weight, and exceptional heat conductivity. On the other hand, alloys that are prone to oxidation, like AlFeSi10Mg, can encourage the development of cavities during the selective laser melting (SLM) process. Consequently, one of the biggest challenges in SLM additive manufacturing (AM) is minimizing porosity. Numerous investigations have been carried out to examine the connection between porosity levels and process factors. These factors consist of hatching distance, scan speed, and laser power. The primary objectives of this study are to comprehend the processes behind pore development during the SLM process and identify strategies for their elimination via process parameter optimization. The density of the components in the SLM process is determined by a number of important design considerations. These variables include the laser's strength, the pace at which the scan is carried out, the thickness of each layer, and the separation between each hatch. Different scanning parameters, laser power levels, and hatching spacings have all been tested by researchers in an effort to minimize porosity and maximize processed component density. Maximizing process development requires a thorough grasp of the production process at every level as well as a rigorous evaluation of several factors. It is important to comprehend the temperature distribution during Selective Laser Melting (SLM) as it has a substantial impact on the final product's density, dimensions, mechanical attributes, and microstructure. Variations in

temperature have the ability to induce residual strain and deformation, which might lead to fractures in the components that are created.

In SLM, thermal deformation is a major worry. It emphasizes how crucial it is to understand process mechanics and parameters in order to enhance SLM. This work aims to examine the effects of porosity and construction orientation on the wear properties of AlFeSi10Mg components produced by selective laser melting (SLM). Through horizontal positioning trials, the study also looks at the expected relationship between wear and flaws, highlighting the effect of a building's alignment on its resistance to wear.

## 2. Materials and Method

### 2.1. Specifications of the sample and AlFeSi10Mg alloy powder

AlFeSi10Mg alloy powder provider SLM Solutions Ltd. is identified in Table 1. This powder is primarily utilised in selective laser melting (SLM) processes, which are common in additive manufacturing. Particle size distribution of the powder ranges from 20 to 63 micrometres ( $\mu\text{m}$ ), ensuring optimal SLM process efficiency. The size range is important because it directly affects the flowability and packing density of the powder, two important characteristics that define the quality of the final printed component. The mechanical characteristics of the printed material are mostly determined by the density of the AlFeSi10Mg powder ( $2.67 \text{ g/cm}^3$ ). The morphology of the samples produced with this powder is I-Section. The rationale for selecting these particular dimensions is to facilitate reliable and consistent mechanical testing. AlSi10Mg alloy components with an I-section form may be selectively laser melted (SLM) to improve heat dissipation, decrease weight, strengthen structural integrity, and simplify manufacturing, among other advantages. During SLM printing, the AlFeSi10Mg powder is uniformly spread into thin layers. Using a high-energy laser and cross-sectional data generated from a 3D model of the product, the powder material is precisely melted. The ideal range for the particle size distribution to provide consistent layer thickness and dependable melting and bonding of powder particles is between 20 and 63  $\mu\text{m}$ . The homogenous nature of the powder and its suitability for the SLM process are shown by the particle size distribution shown in Figure 1. Precise control over the powder bed and laser enables accurate and consistent component production, ensuring that the final products meet strict quality requirements.

**Table 1.** Chemical composition of AlFeSi10Mg alloy

ELEMENT	Wt(grams)
Mg	0.45
Al	69.64
Si	9.9
Cr	0.79
Fe	0.55
Cu	0.05
<b>Total</b>	<b>81.62</b>

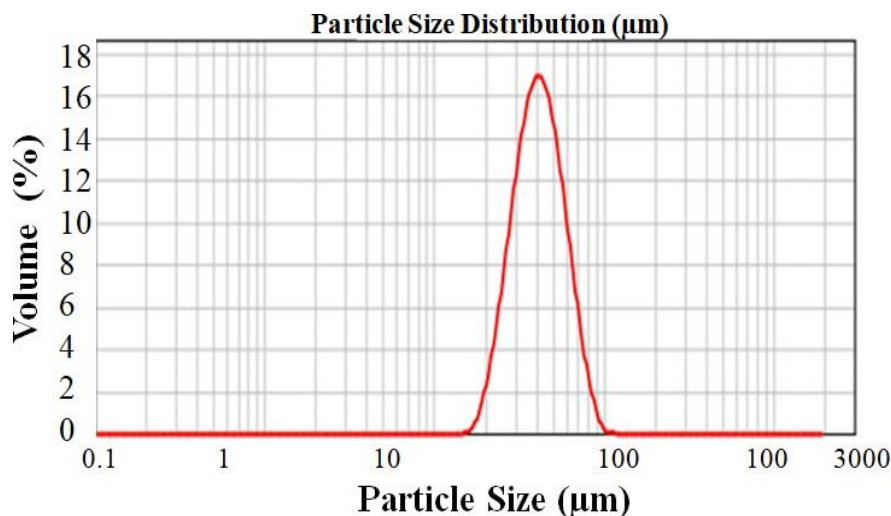


**Figure 1:** Powder particle size distribution

### 2.2 SLM Procedure

This investigation's AlFeSi10Mg alloy samples were produced using a German-manufactured SLM Solutions M280 2.0 Laser Powder Bed Fusion (L-PBF) apparatus. The apparatus, seen in Figure 2a, operates on a 400 watt continuous-wave Yb-fiber laser inside an argon gas environment. Due to its enormous volume capacity

of  $280 \times 280 \times 365 \text{ mm}^3$ , the SLM M280 build platform may be used to create large parts or several smaller components at the same time. A few tweaks are needed while using the Selective Laser Melting (SLM) method. These qualities are essential and might significantly affect the calibre of the finished product. Comprehending these procedural elements is essential for achieving effective model training and energy optimisation. Our model's inputs consist of four essential elements. A more thorough description of these elements may be found here:

The procedure is affected by the following variables: layer thickness, hatching distance, scan speed, and laser power.

The laser intensity is a critical factor that directly influences the energy absorbed during the dissolving of the material. As a result of incorrect calibration and excessive power consumption, the final product is characterised by defects and porosity that result from the irregular melting of the material. Nevertheless, an excessively high laser power may lead to insufficient heat dispersion, which could accumulate excess heat and cause severe burning. SLM apparatus typically employ lasers with a power range of 200–1,000 W. Scanning Speed: The scan velocity is a critical factor in the SLM sintering procedure. The flow is altered, and the output quality is ultimately reduced, as the molten pool contracts more rapidly than the scan speed. The ejection of molten pool particles may result from an increase in scanning velocity, which could result in the formation of gas-filled cavities, partial fusion, and microstructure abnormalities. As a result, it is essential to select the appropriate scanning velocity in order to generate a densely packed and consistent structure. The seam spacing is a critical factor in the regulation of the density and surface quality of products produced by Selective Laser Melting (SLM). The measurement is conducted by calculating the distance between the foci of parallel laser beam trajectories. The production rates are immediately influenced by the increased laser layer scanning that results from an increase in hatch distance.

However, denser layers necessitate a larger laser point size due to the necessity of a shorter hatch distance. Insufficient hatching spacing may result in spaces between images, which would render the object's structure permeable. It is crucial to achieve equilibrium, as an excessively large hatch spacing may result in high porosity and substandard materials. The primary focus of the research is hatch spacing, as it significantly influences the density, construction speed, and overall quality of the components that are produced. The millimetre measuring range is 0.05 mm to 0.25 mm.

The vertical distance between consecutive layers in additive manufacturing methods, such as selective laser melting (SLM), is called the layer thickness. It significantly affects the final product's surface's overall quality, intricacy, and smoothness. Thicker layers provide smoother surfaces and more precise features, but they may take longer to print. Thinner layers may speed up printing, but they may also reduce smoothness and detail in the final product. The selection is influenced by the machine's capabilities, special demands, material, and application. The layer separation must be between 0.02 and 0.1 mm. This coefficient displays the production rate in cubic metres per hour. Cubic centimetres per hour, abbreviated as  $\text{cm}^3/\text{h}$ . To guarantee consistency across all samples throughout the printing process, a set of constants was kept in addition to the variable values shown in Table 2. Maintaining the build platform at  $1500^\circ\text{C}$  to provide a steady temperature environment for printing was one of the constants. By keeping the laser spot diameter constant at 75 micrometres ( $\mu\text{m}$ ), a perfect focus point for the laser to generate accurate melting and bonding of the powder particles was guaranteed. A consistent piece density and uniform layer deposition were guaranteed by keeping the layer thickness at 30  $\mu\text{m}$ . The scanning orientation remained at  $0^\circ$  (horizontal direction) at the end of the specimen production process, indicating that no further support structures were required. With the fixed settings in place, a uniform printing process was achieved, ensuring reliable and consistent results for all printed samples.

### 2.3. Conducting Experiments

By employing an L16 orthogonal array and the design of experiments (DOE) approach, the process parameters were established. This technique enables a systematic analysis of the effects of different parameter combinations on the final printed components. The specimens were printed horizontally at a  $0^\circ$  angle and did not need any additional support structures. The maximum oxygenation of the gas during the SLM printing process reached approximately 0.12%. Maintaining low oxygen levels is crucial in order to prevent powder oxidation, which could have a detrimental effect on the mechanical properties and surface finish of printed objects. This calculation enhances our understanding of the relationship between energy input and the bonding and merging of the powder particles.

Figure 2b presents accurate energy density measurements for each test condition (T1 through T15). The worn samples displayed in Figure 3 were subjected to a series of tests to assess their durability and mechanical characteristics.

Deliberate change of process parameters inspired by test design allowed for a thorough examination of optimal configurations for using the SLM technology to make high-quality AlFeSi10Mg components. To sum

up, the production of trustworthy and excellent AlFeSi10Mg alloy samples that were then used for wear and mechanical testing was made possible by the meticulous control of process variables and the rigorous experimental design.

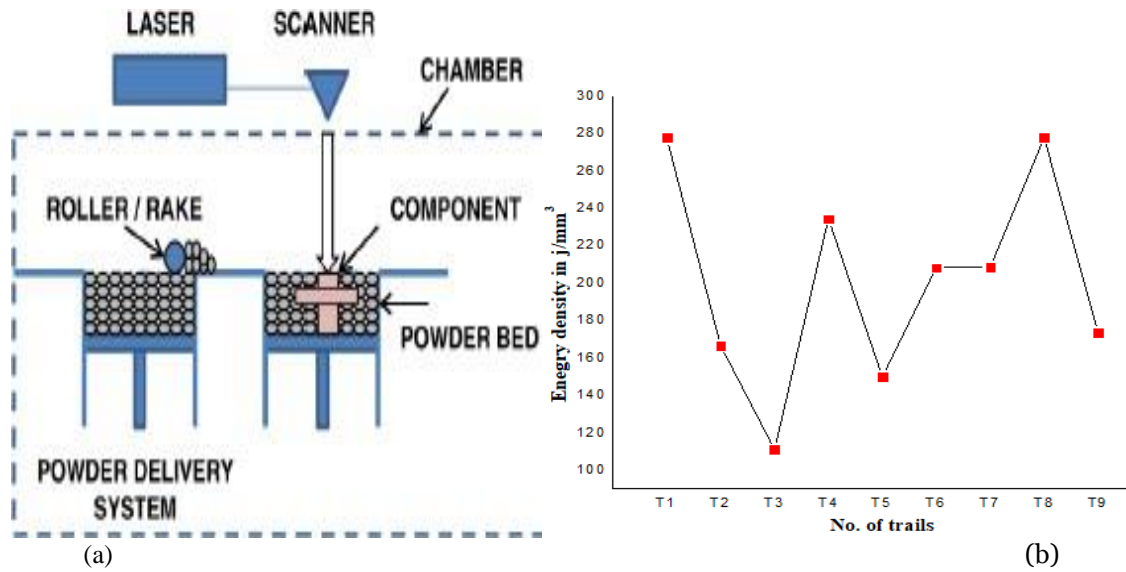


**Figure 2:** a) SLM schematic diagram and b) laser energy density results.

**Table 2:** Experimental Observations

Run	A: power watt	B: Speed mm/sec	C: Hatching Distance H mm	D- Layer thickness T mm	R1 LED j/mm	R2 SED j/mm <sup>2</sup>	R3 VED j/mm <sup>3</sup>
T1	370	900	0.173	0.04	0.411	2.38	59.41
T2	370	1300	0.25	0.02	0.284	1.14	56.92
T3	370	1235	0.1	0.04	0.3	3	74.9
T4	370	1270	0.15	0.05	0.291	1.94	38.85
<b>T5</b>	<b>370</b>	<b>955</b>	<b>0.15</b>	<b>0.02</b>	<b>0.387</b>	<b>2.58</b>	<b>129.14</b>
T6	370	1300	0.25	0.02	0.284	1.14	56.92
T7	370	1270	0.15	0.03	0.291	1.94	64.74
T8	325	1100	0.25	0.03	0.295	1.18	39.39
T9	295	1300	0.125	0.06	0.226	1.82	30.26
T10	317	1000	0.25	0.04	0.317	1.27	31.7
T11	314	900	0.199	0.06	0.348	1.75	30.16
T12	295	1100	0.125	0.03	0.268	2.15	71.52
T13	310	1270	0.25	0.05	0.244	0.98	19.58
T14	325	1250	0.25	0.04	0.26	1.04	26
T15	325	1300	0.15	0.03	0.25	1.67	55.56

### 3. Results and Discussion

#### 3.1 Microstructure Evaluation

Figures 3a, 3b, and 3c show how the microstructure of the AlFeSi10Mg alloy samples was analysed at various magnification levels using a scanning electron microscope (SEM). The SEM images provide detailed views of the samples' internal structure and surface appearance, highlighting significant information that influences the mechanical characteristics of the material. The micrographs demonstrate differences in the microstructure depending on which processing parameters were used during the SLM printing process. Figures 3d, 3e, and 3f illustrate notable defects in materials produced with low laser power in conjunction with certain scan speeds (T1, T2, and T3), including porosity, oxide coatings, and fractures. These flaws result from inadequate fusion and bonding between the powder particles due to insufficient energy input. Differences in the melting process are shown by the occurrence of both round and irregular holes. Furthermore, thermal stresses and a lack of affinity between oxides and the metal matrix may be to blame for the presence of horizontal fractures inside the structure. This leads to the development and spread of long-term surface cracks.

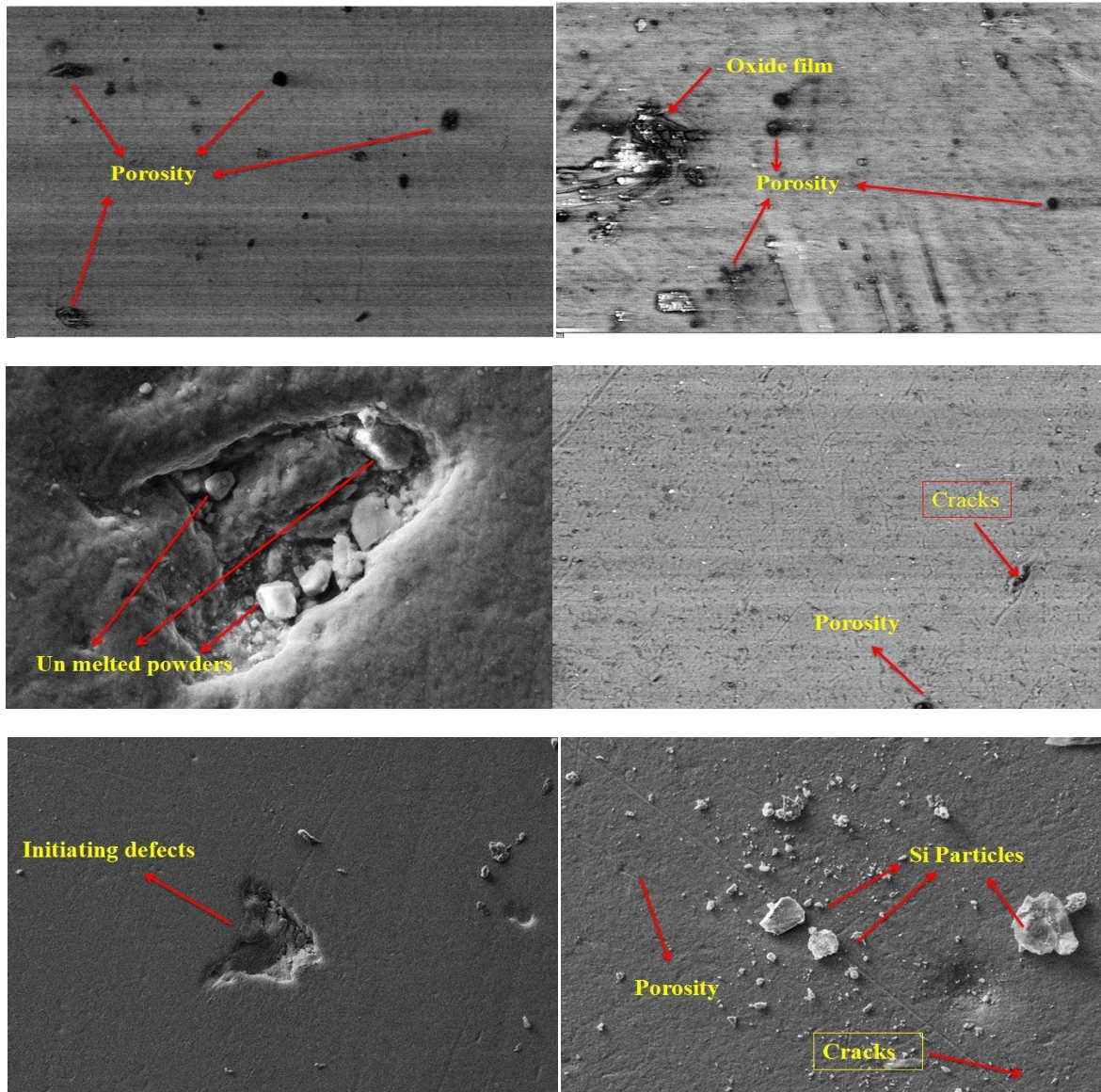


**Figure 3.** Defects at different laser power and scan rates a) 370 watts with 1300mm/s, b) 370watts with 1270 mm/s, c) 325 watts with 1000 mm/s, d) 370watts with 955 mm/s, e) 314 watts with 900 mm/s, and f) 325 watts with 1300 mm/s.

Thermal deviations were seen when more laser power was applied at certain scan rates (T13, T14, and T15). These findings suggest that problems such as residual stresses and warping might be the consequence of overheating. The delayed cooling rate of the process led to the development of oxidation on certain AlFeSi10Mg powder particles, which in turn compromised the structural integrity of the printed components. The study discovered that the distance at which hatching occurs is a significant factor affecting the strength and functioning of the printed samples. Changes in the hatching distance had an impact on the components' hardness and density. More precisely, when the laser's power dropped, density and hardness also dropped. On the other hand, a faster scan speed led to a higher hardness but a lower density because more pores developed.

Based on the principles of experimental design, the samples generated under the specific conditions of T5 were of higher quality and had fewer mistakes. Figure 5 illustrates the enhanced microstructure of the samples obtained under these ideal conditions at various magnification settings. Conversely, samples generated under T4 and T6 conditions exhibited porosity and fractures, mostly as a result of insufficient cooling rates and sluggish scan speeds.

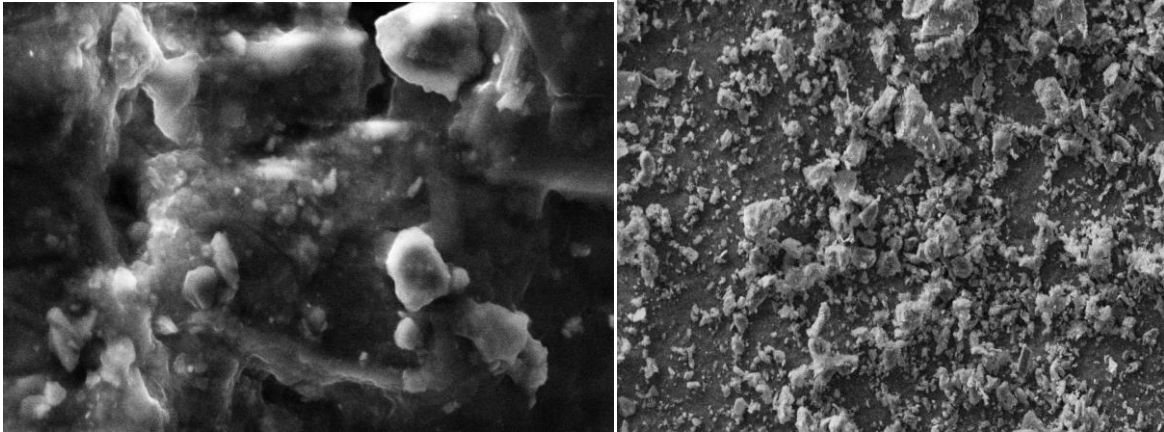


**Figure 4:** (a and b) Defects free components microstructure at T5 as 370 watts with 955 mm/s.

The AlFeSi10Mg alloy samples' microstructure was examined at various magnification settings using a scanning electron microscope (SEM). The outcomes are shown in figures 3a, 3b, and 3c. The SEM images provide detailed views of the internal structure and surface appearance of the samples, with an emphasis on critical properties that influence the material's mechanical capabilities. The micrographs demonstrate how the processing settings used in the SLM printing process impact the microstructure. The samples generated by combining low laser power with certain scan speeds (T1, T2, and T3) contain noticeable flaws such as porosity, oxide coatings, and fractures, as shown in Figures 3d, 3e, and 3f. These defects result from inadequate fusion and bonding of the powder particles due to insufficient energy input. More precisely, the uneven melting process is suggested by the presence of both round and irregular holes. In addition, longitudinal cracks occur and spread across the surface due to the combination of limited wettability between oxides and the metal matrix and heat stresses. This is the main cause of the fractures that occur in the structure's horizontal direction. Thermal variations were observed at different scan speeds (T7, T8, and T9) while using a greater laser power. According to these results, overheating could be the source of warping and residual stresses. Due to the insufficient cooling rate during the procedure, certain particles of the AlFeSi10Mg powder underwent oxidation, which posed a risk to the overall integrity of the printed pieces. Based on the experiment's findings, it was observed that the distance at which the samples were hatched had a significant impact on their strength and usefulness. The toughness and density of the fragments were influenced by variations in distance during the hatching process. Specifically, as the laser intensity decreased, so did the density and hardness. However, as the scan speed increased, pores began to form, resulting in higher density but lower hardness.

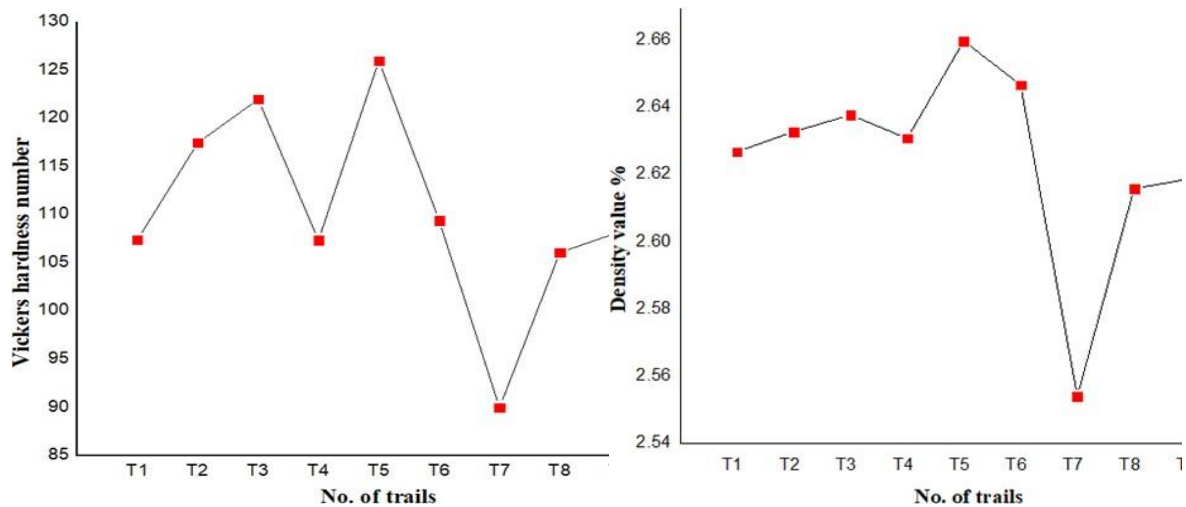
Under certain conditions (T5), samples produced following the principles of experimental design (DoE) showed a decrease in flaws and an enhancement in quality. The samples in Figure 4 exhibit superior microstructure when viewed at different magnification levels, which can be attributed to fortuitous circumstances. However, samples created using the T4 and T6 parameters exhibited porosity and fractures, primarily due to inadequate cooling rates and scan speeds. The microstructural characterisation had a significant impact on the mechanical characteristics of the samples, specifically their strength and hardness. Understanding the relationship between scan speed and laser power is crucial for achieving optimal microstructure and flawless product quality. The study's conclusion highlights the significance of processing variables in determining the final characteristics of the AlFeSi10Mg alloy component produced through selective laser melting (SLM) printing.

### 3.2 Density and Hardness

The hardness and density of the AlFeSi10Mg alloy samples were evaluated using the L16 orthogonal array design of experiments (DoE), the results of which are shown in Table 6. The hardness testing was carried out in accordance with the ASTM E384 standard using the Vickers hardness test method. Each of the fifteen samples was subjected to microhardness testing, which yielded the Vickers hardness value by making three indentations at three separate sites on each specimen. Sample T5 achieved a maximum hardness value of  $126 \pm 5$  HV after loading 1000 grammes into it and allowing it to rest for 10 seconds at each indentation site. In compliance with the ASTM SI 10 standard, the Archimedes technique was used to ascertain the substance's density. The theoretical density ( $\rho_t$ ) of the AlFeSi10Mg alloy powder is  $2.67 \text{ g/cm}^3$ . The highest density attained in the manufactured components, especially for sample T5, was  $2.66 \text{ g/cm}^3$ , according to the post-SLM study. This measurement shows that components with densities that are very near to the predicted value may be produced by optimisation of the SLM process. This implies that the components have extremely minimal porosity and imperfections.

**Table 3.** Mechanical properties of density and hardness.

Trail No.	Hardness (HV)	Density (%)
T1	106.44	2.62 (98.3%)
T2	123.13	2.633 (98.6%)
T3	120	2.638 (98.8%)
T4	102.35	2.61 (98.5%)
T5	124	2.650 (99.6%)
T6	108.4	2.647 (99.1%)
T7	89	2.554 (95.6%)
T8	104.8	2.616 (97.9%)
T9	107.24	2.61 (98.0%)

**Figure 5:** a) Vickers hardness and b) Density of AlFeSi10Mg samples.

Hardness and density are only two of the mechanical qualities that are greatly influenced by the microstructural characteristics, which include the existence of pores, fissures, and overall porosity. Because of the higher energy densities, samples are more prone to keyholing when utilising high laser power and low scan speed. Temperature variations and a rise in porosity follow as a consequence. Decreases in hardness and density readings are the outcome of these flaws. On the other hand, the ideal configurations—especially the ones used for sample T5—minimize these flaws to the absolute minimum, producing exceptional mechanical characteristics. It is evident from the data in Figure 5 and Table 3 that increasing the laser power from 300 to 370 watts and the scan speed from 900 to 1300 mm/s causes a significant drop in hardness and density. More precisely, the hardness drops from  $126 \pm 5$  HV to  $90 \pm 5$  HV, and the density drops from 99.6% to 95.6% of the theoretical value. This trend highlights how important it is to strike a balance between scan speed and laser power in order to get the best material properties. Sample t5 shows that the right mix yields good results with high hardness and density values, which suggest fewer internal defects and a strong microstructure. In conclusion, our research emphasises the importance of precise control over the SLM process parameters in order to maximise the mechanical properties of components fabricated from the AlFeSi10Mg alloy. Understanding the connection between process variables, structural integrity, and mechanical properties is crucial when utilising additive manufacturing techniques to create delicate components.

### 3.3 Wear Characterization

When studying the friction properties of AlFeSi10Mg alloy samples, it is important to analyse two key factors: the wear rate and the coefficient of friction. The experiment analysed nine samples that were subjected to various process conditions using an L16 orthogonal array. Figure 7 shows the rate of deterioration of the AlFeSi10Mg material at different sliding speeds. This experiment demonstrates the wear rate under specific conditions: a sliding speed of 300 rpm, a constant load of 60 N, and an operating time of 300 seconds.

The results show that under these conditions, intrinsic material faults such as porosity and pores—which are affected by certain SLM process parameters—increase the rate of wear of AlFeSi10Mg.

Fifteen samples were produced and made using the design of experiments and the SLM methodology, as shown in figure 6. The sliding distance was 80 mm, and the experimental tests were carried out under isothermal circumstances at a constant ambient temperature of 25°C. After trials T1 through T9 were finished, sample T5 showed the best outcomes. The sample performed quite well, as the curve in Figure 10 illustrates.



**Figure 6:** Fabricated specimens with SLM

A thorough examination of sample t5's findings is shown in Table 4, where 94 micrometres of damage is the least amount of damage found. The volume of wear was measured at 1.25 mm<sup>3</sup>, but the change in length had a negligible value of 0.06%. In addition, the wear rate was determined to be  $4.97 \times 10^{-8}$  mm<sup>2</sup>/N, whereas the wear velocity was measured at 1674.46 mm/s. The frictional force was found to be 14.1 N, and the wear coefficient was found to be 0.04 mm<sup>2</sup>/N. The results showed that sample T5 performed better in terms of wear resistance and friction than the other samples that were evaluated. Figure 9 illustrates the variations in wear and frictional force among the samples. The samples with more obvious cracks, porosity, and other SLM processing flaws had the highest amount of wear-induced material loss. It has been shown that raising the laser's power and scan speed led to higher wear and friction rates, which might be a sign of more significant material or manufacturing issues. These findings highlight the need of optimising the settings of the selective laser melting (SLM) process in order to decrease defects, enhance wear resistance, and increase overall functioning of components composed of the AlFeSi10Mg alloy.



**Figure 7:** (a and b) Wear testing schematic diagram.

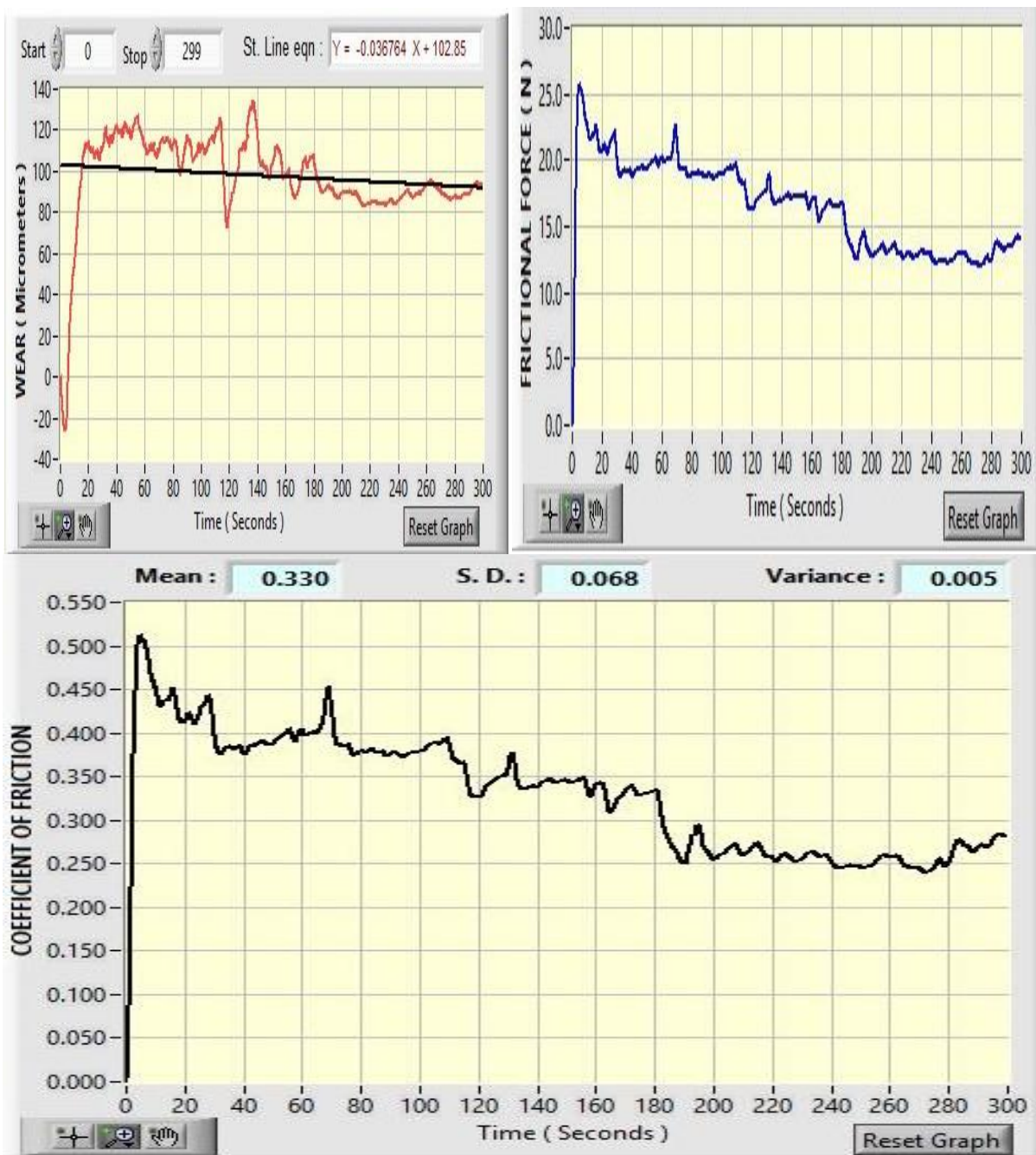
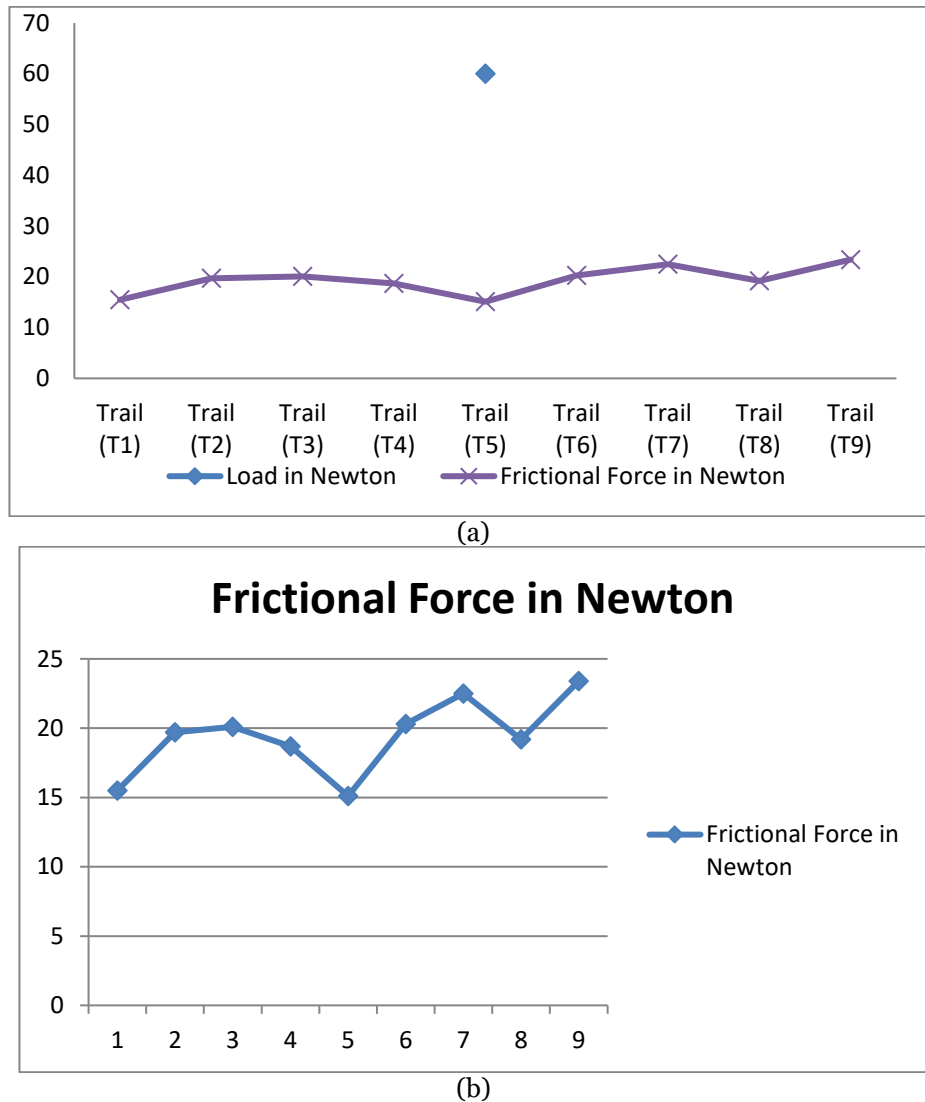


Figure 8: (a) wear, (b) frictional, and (c) coefficient friction results

Table 4: Wear and frictional results

No. of Trails	Load in Newton	Speed in rpm	Time in minutes	Wear in Micrometer	Frictional Force in Newton
Trail (T1)				167	15.5
Trail (T2)				210	19.7
Trail (T3)				399	20.1
Trail (T4)				567	18.7
Trail (T5)	60	300	7	97	15.1
Trail (T6)				555	20.3
Trail (T7)				598	22.5
Trail (T8)				652	19.2
Trail (T9)				734	23.4



**Figure 9:** a) wear characterization results and b) Frictional force results.

#### 4. Conclusion

As a result, this study clarifies the selective laser melting (SLM) process that is used to produce AlFeSi10Mg alloy parts. The approach is mainly focused on wear assessment and fault analysis. The study emphasises the importance of building orientation via careful analysis and rigorous testing, especially in relation to wear behaviour. The mechanical characteristics of printed items may be enhanced and the quantity of mistakes can be decreased by carefully adjusting the construction orientation. The study shows how important process variables, such as scan speed and laser power, are to the quality of printed products. It has been shown that higher laser powers and scan speeds result in more defects like porosity, pores, and cracks, which lower wear resistance, fatigue strength, density, and hardness.

By carefully changing process parameters—that is, by employing low laser power and lowering scan speeds—defect-free components can be optimised. Using this method reduces defects and results in distortion-free components. A 370 Watt laser power, a 955 mm/s scan speed, and a 0.1  $\mu\text{m}$  hatching spacing are among the exact requirements for optimal performance that the study sets forth. Reduced fault occurrence and improved mechanical properties result from these parameters. Excellent mechanical properties were shown by the AlFeSi10Mg alloy components at the optimum values. The following characteristics are included: a wear rate of 94 micrometres, a change in length of 0.06%, a wear volume of 1.25  $\text{mm}^3$ , a wear velocity of 1674.46 mm/s, a wear coefficient of 0.04  $\text{mm}^2/\text{N}$ . The obtained hardness of  $126 \pm 5$  HV and density of 2.66 (99.6%) are proof that the optimised SLM technique is effective in producing high-quality components. The industrial applicability of the findings of this work are highly significant, particularly in those industries that use components made of AlFeSi10Mg alloy. Manufacturers that understand and optimise the SLM process parameters can obtain components with better mechanical properties, fewer defects, and improved performance. More dependability and efficiency follow from this in a variety of applications.

### Acknowledgment:

We sincerely thank the reviewers who stayed anonymous for their thoughtful feedback.

### Data Availability:

We thus certify that all of the information in this text is original to us and has not been obtained from other sources.

### Conflict of Interest:

The authors state that there are no conflicts of interest related to this study.

### Ethics Approval:

The described research, according to the authors, was unaffected by competing financial or personal interests.

### Consent to Participate:

All writers willingly participated to this research project at their own discretion.

### Consent for Publication:

The authors give the journal their consent to publish this study.

### References

1. Aboulkhair NT, Maskery I, Tuck C, Ashcroft I, Everitt NM. The microstructure and mechanical properties of selectively laser melted AlSi10Mg: The effect of a conventional T6-like heat treatment. *Materials Science and Engineering: A*. 2016, 667, 139-46.
2. Gu D, Wang H, Dai D, Chang F, Meiners W, Hagedorn YC, Wissenbach K, Kelbassa I, Poprawe R. Densification behavior, microstructure evolution, and wear property of TiC nanoparticle reinforced AlSi10Mg bulk-form nanocomposites prepared by selective laser melting. *Journal of Laser Applications*. 2015 Feb 9;27(S1):S17003.
3. Nirish M, Rajendra R. Suitability of metal additive manufacturing processes for part topology optimization—A comparative study. *Materials Today: Proceedings*. 2020, 27, 1601-7.
4. Zou J, Zhu Y, Pan M, Xie T, Chen X, Yang H. A study on cavitation erosion behavior of AlSi10Mg fabricated by selective laser melting (SLM). *Wear*. 2017 Apr 15;376:496-506.
5. Wu L, Zhao Z, Bai P, Zhao W, Li Y, Liang M, Liao H, Huo P, Li J. Wear resistance of graphene nanoplatelets (GNPs) reinforced AlSi10Mg matrix composite prepared by SLM. *Applied Surface Science*. 2020 Feb 15;503:144156.stress”, *International Journal of Fatigue*, vol.138, pp.105696, 2020.
6. Larrosa NO, Wang W, Read N, Loretto MH, Evans C, Carr J, Tradowsky U, Attallah MM, Withers PJ, “Linking microstructure and processing defects to mechanical properties of selectively laser melted AlSi10Mg alloy”, *Theoretical and Applied Fracture Mechanics*, vol.98, pp.123-33, 2018.
7. Mower TM, Long MJ, “Mechanical behavior of additive manufactured, powder-bed laser-fused materials”, *Materials Science and Engineering: A*, vol. 651, pp.198-213, 2016.
8. Maamoun AH, Xue YF, Elbestawi MA, Veldhuis SC. Effect of selective laser melting process parameter on the quality of all alloy parts: Powder characterization, density, surface roughness, and dimensional accuracy. *Materials*. 2018, 11(12), 2343.
9. Wu H, Ren Y, Ren J, Cai A, Song M, Liu Y, Wu X, Li Q, Huang W, Wang X, Baker I. Effect of melting modes on microstructure and tribological properties of selective laser melted AlSi10Mg alloy. *Virtual and Physical Prototyping*. 2020 Dec 8;15(sup1):570-82.
10. Wang P, Gammer C, Brenne F, Prashanth KG, Mendes RG, Rümmele MH, Gemming T, Eckert J, Scudino S. Microstructure and mechanical properties of a heat-treatable Al-3.5 Cu-1.5 Mg-1Si alloy produced by selective laser melting. *Materials Science and Engineering: A*. 2018, 10, 711, 562-70.
11. Li R, Chen H, Zhu H, Wang M, Chen C, Yuan T. Effect of aging treatment on the microstructure and mechanical properties of Al-3.02 Mg-0.2 Sc-0.1 Zr alloy printed by selective laser melting. *Materials & Design*. 2019, 168, 107668.
12. Dai D, Gu D, Xia M, Ma C, Chen H, Zhao T, Hong C, Gasser A, Poprawe R. Melt spreading behavior, microstructure evolution and wear resistance of selective laser melting additive manufactured AlN/AlSi10Mg nanocomposite. *Surface and Coatings Technology*. 2018 Sep 15;349:279-88.
13. Yu T, Liu J, He Y, Tian J, Chen M, Wang Y. Microstructure and wear characterization of carbon nanotubes (CNTs) reinforced aluminum matrix nanocomposites manufactured using selective laser melting. *Wear*. 2021 Jul 15;476:203581.
14. Hamidi Nasab M, Giussani A, Gastaldi D, Tirelli V, Vedani M. Effect of surface and subsurface defects on fatigue behavior of AlSi10Mg alloy processed by laser powder bed fusion (L-PBF). *Metals*. 2019, 9(10), 1063.

15. Park TH, Baek MS, Sohn Y, Lee KA. Effect of post-heat treatment on the wear properties of AlSi10Mg alloy manufactured by selective laser melting. *Archives of Metallurgy and Materials*. 2020;65.
16. Bajaj P, Wright J, Todd I, Jäggle EA. Predictive process parameter selection for Selective Laser Melting Manufacturing: Applications to high thermal conductivity alloys. *Additive Manufacturing*. 2019, 27, 246-58.
17. Wei P, Chen Z, Zhang S, Fang X, Lu B, Zhang L, Wei Z. Effect of T6 heat treatment on the surface tribological and corrosion properties of AlSi10Mg samples produced by selective laser melting. *Materials Characterization*. 2021 Jan 1;171:110769.
18. Zhuo L, Wang Z, Zhang H, Yin E, Wang Y, Xu T, Li C. Effect of post-process heat treatment on microstructure and properties of selective laser melted AlSi10Mg alloy. *Materials Letters*. 2019 Jan 1;234:196-200.
19. Wang P, Lei H, Zhu X, Chen H, Fang D, "Influence of manufacturing geometric defects on the mechanical properties of AlSi10Mg alloy fabricated by selective laser melting", *Journal of Alloys and Compounds*. Vol.789, pp.852-9, 2019.
20. Aboulkhair NT, Maskery I, Tuck C, Ashcroft I, Everitt NM, "The microstructure and mechanical properties of selectively laser melted AlSi10Mg: The effect of a conventional T6-like heat treatment", *Materials Science and Engineering: A*, vol.667, pp.139-46, 2016.
21. Read N, Wang W, Essa K, Attallah MM, "Selective laser melting of AlSi10Mg alloy: Process optimisation and mechanical properties development", *Materials & Design*, vol.65, pp.417-24, 2015.
22. Nirish M, Rajendra R. Effect of Heat Treatment on Wear Characterization of AlSi10Mg Alloy Manufactured by Selective Laser Melting. *Journal of mechanical engineering research and development*. 9:11-00.
23. Nirish M, Rajendra R. Heat Treatment Effect on the Mechanical Properties of AlSi10Mg Produced by Selective Laser Melting. *Journal of mechanical engineering research and development*. 9:11-00.
24. Nirish M & Rajendra R. Optimization of Process Parameter and Additive Simulation for Fatigue Strength Development by Selective Laser Melting of AlSi10Mg Alloy. *International Journal of Mechanical Engineering*. Vol.7 (2). ISSN: 0974-5823. pp.3795-3802.2022.
25. Bai P, Huo P, Kang T, Zhao Z, Du W, Liang M, Li Y, Liao H, Liu Y, "Failure Analysis of the Tree Column Structures Type AlSi10Mg Alloy Branches Manufactured by Selective Laser Melting", *Materials*, vol.13, no.18, pp.3969, 2020.
26. Wang P, Lei H, Zhu X, Chen H, Fang D. Influence of manufacturing geometric defects on the mechanical properties of AlSi10Mg alloy fabricated by selective laser melting. *Journal of Alloys and Compounds*. 2019, 789, 852-9.
27. Ferro P, Meneghello R, Razavi SM, Berto F, Savio G. Porosity inducing process parameters in selective laser melted AlSi10Mg aluminium alloy. *Physical Mesomechanics*. 2020, 23(3), 256-62.
28. Liu Y, Liu C, Liu W, Ma Y, Tang S, Liang C, Cai Q, Zhang C. Optimization of parameters in laser powder deposition AlSi10Mg alloy using Taguchi method. *Optics & Laser Technology*. 2019, 111, 470-80.
29. Read N, Wang W, Essa K, Attallah MM. Selective laser melting of AlSi10Mg alloy: Process optimisation and mechanical properties development. *Materials & Design*. 2015, 65, 417-24.
30. Wu H, Li J, Wei Z, Wei P. Effect of processing parameters on forming defects during selective laser melting of AlSi10Mg powder. *Rapid Prototyping Journal*. 2020.
31. Oliveira JP, LaLonde AD, Ma J. Processing parameters in laser powder bed fusion metal additive manufacturing. *Materials & Design*. 2020, 193, 108762.
32. Samantaray M, Thatoi DN, Sahoo S. Modeling and optimization of process parameters for laser powder bed fusion of AlSi10Mg alloy. *Lasers in Manufacturing and Materials Processing*. 2019, 6(4), 356-73